Electrocatalysis

DOI: 10.1002/anie.200604732

In Situ Time-Resolved Dynamic Surface Events on the Pt/C Cathode in a Fuel Cell under Operando Conditions**

*Mizuki Tada, Shigeaki Murata, Takahiko Asakoka, Kazutaka Hiroshima, Kazu Okumura, Hajime Tanida, Tomoya Uruga, Haruyuki Nakanishi, Shin-ichi Matsumoto, Yasuhiro Inada, Masaharu Nomura, and Yasuhiro Iwasawa**

Environment-friendly proton-exchange-membrane fuel cells (PEMFC) are considered a possible answer to environmental and energy problems.[1–8] To make fuel-cell automobiles a reality, the activity and life of the Pt/C cathode catalyst must be improved. Towards this goal, we have developed a novel time-gating quick XAFS (QXAFS) technique with 1-s time resolution and an energy-dispersive XAFS (DXAFS) system with 4-ms time resolution. Using these techniques, we have observed the electrochemical reaction mechanism and found evidence for dynamic surface events involving Pt dissolution at the Pt/C cathode, the reaction kinetics of the electron-transfer processes, redox structural changes (eight elementary steps), and a significant time lag among those events for the first time under operando fuel-cell conditions.

Measurement of the current in a PEMFC in real time shows that a power-on process from open circuit to an operating state brings about rapid electrochemical reactions on its electrode surfaces, which are completed within a few seconds. Such power-on and -off processes (voltage change from open-circuit voltage (OCV = e.g. 1.0 V) to operating voltage (e.g. 0.4 V)) with huge energy transfer are indispensable for commercial applications of fuel-cell systems. However, surface atoms of the active metal particles tend to dissolve slightly into the electrolyte that is in contact with the cathode catalyst layer, and an undesired Pt particle (or layer) deposits in the electrolyte.[9,10] This effect is a problem because automobiles, in particular, require continual repetition of the on/off processes with rapid changes in cell voltages to alter the car's speed.

To overcome these serious problems, reaction mechanisms on the electrode surfaces must be investigated in situ during voltage-stepping processes in real time. However, to the best of our knowledge, there are no reports that have fully explored and determined the reaction kinetics of both the structural changes of the metal catalysts and the electrochemical reactions on the electrode surfaces in PEMFCs. We have investigated the mechanism of the electrochemical processes involved in rapid voltage-controlled processes on a Pt/C catalyst. From the viewpoints of electrification and structural changes in the Pt catalyst, in situ time-resolved quick X-ray absorption fine structure (QXAFS) spectroscopy was used to monitor directly the chemical bonding and electronic states in the Pt nanoparticles that act as the electrodes.[11–17]

Acquisition of a QXAFS spectrum at a Pt L_{III} edge requires at least 15 s because of the slow mechanical rotation of the monochromator; however, the time resolution (15 s) is too slow to observe the reaction mechanism of the target processes. Herein, we propose a novel time-gating quick XAFS (TG-QXAFS), with 1-s time resolution, for the first time. The in situ TG-QXAFS measurements of the potential stepping processes in real time revealed extraordinary time lags between electrification and the redox chemical processes on the Pt nanoparticles at the fuel-cell cathode, which are relevant to the overall reaction mechanism at the cathode under true fuel-cell operation conditions.

Figure 1 and the Supporting Information show a schematic of the new TG-QXAFS apparatus and the measurement procedure. The system is synchronized with a potentiostat connected to a homemade electrode XAFS cell (Figure 1b). Membrane–electrode assemblies (MEAs) containing Pt/C as a cathode catalyst and Pt-free Pd/C as an anode catalyst were stacked between two current collectors containing graphite flow fields, illustrated in Figure 1c. X-rays pass through a small hole made in the center of the XAFS cell, and the MEA is pinched between the two flow fields. A

[*] Dr. M. Tada, Prof. Dr. Y. Iwasawa
Department of Chemistry, Graduate School of Science
The University of Tokyo
Hongo, Bunkyo-ku, Tokyo 113-0033 (Japan)
Fax: (+81) 3-5800-6892
E-mail: iwasawa@chem.s.u-tokyo.ac.jp
S. Murata, Dr. H. Nakanishi, Dr. S.-i. Matsumoto
Fuel Cell System Development Center
Toyota Motor Corporation
1200, Mishiku, Susono, Shizuoka 410-1193 (Japan)
T. Asakoka, K. Hiroshima
Toyota Central R&D Labs. Inc.
Nagakute, Aichi 480-1192 (Japan)
Dr. K. Okumura
Department of Materials Science, Faculty of Engineering
Tottori University
Koyama-cho, Tottori 680–8552 (Japan)
Dr. H. Tanida, Dr. T. Uruga
Japan Synchrotron Radiation Research Institute
Kouto, Sayo-cho, Sayo-gun, Hyogo 679-5198 (Japan)
Dr. Y. Inada, Prof. Dr. M. Nomura
Photon Factory, Institute of Materials Structure Science
High Energy Accelerator Research Organization (KEK)
Tsukuba, Ibaraki 305-0801 (Japan)

[**] This work has been performed with the approval of SPring-8 (Proposal No. 2005A0451-NXa-np) and PF PAC (Proposal No. 2005G207).

Supporting information for this article is available on the WWW under http://www.angewandte.org or from the author.

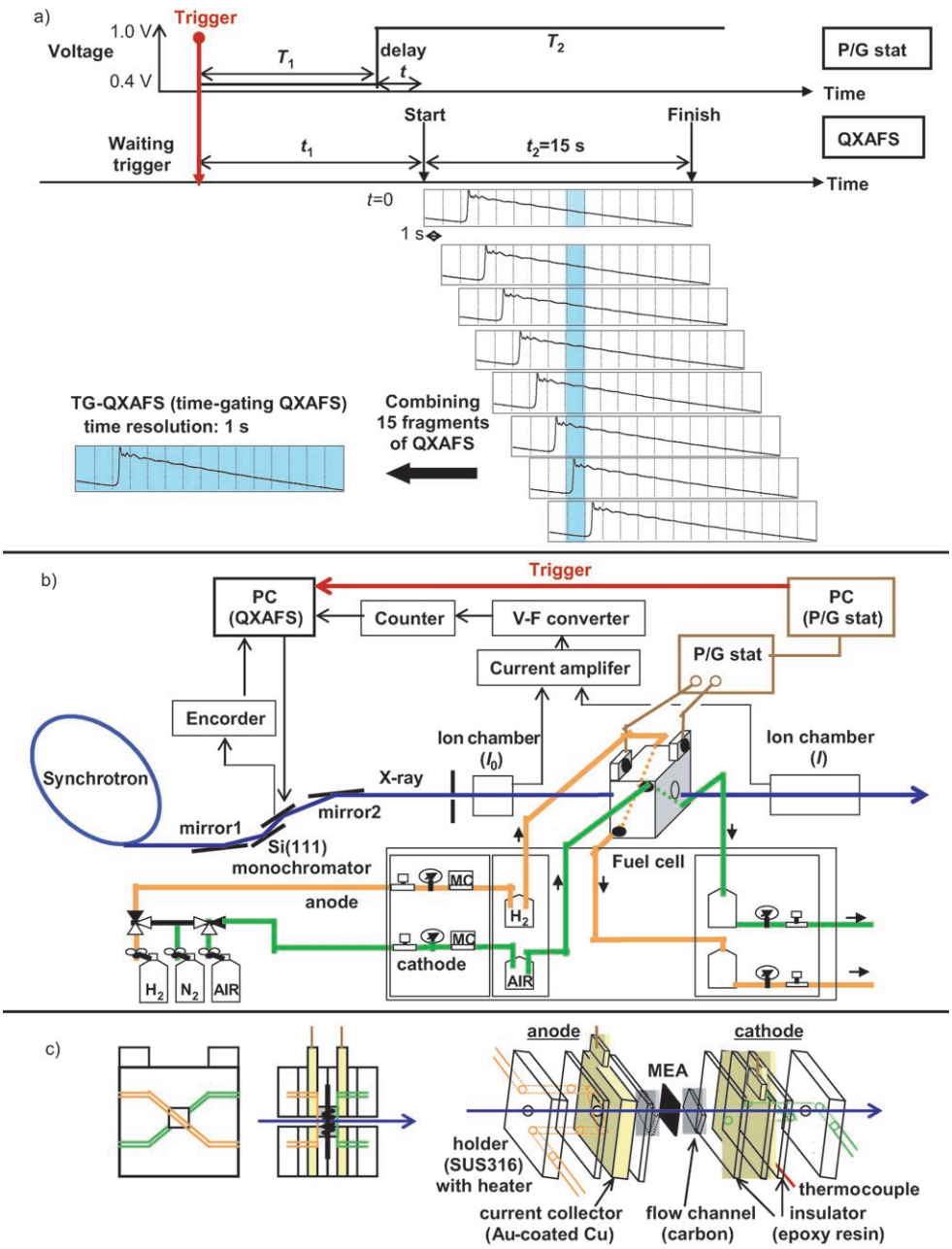

Figure 1. a) The procedure for TG-QXAFS measurements with a time resolution of 1 s. b) A schematic of the fuel cell and the in situ time-resolved TG-QXAFS system at SPring-8 BL01 station. The potentiostat and QXAFS system were synchronized, and a trigger signal was sent from the potentiostat to the QXAFS system. c) In situ XAFS fuel cell. Orange line: H_2 inlet for the anode; green line: N_2 or air inlet for the cathode.

trigger signal is sent from the potentiostat to the QXAFS system, and time zero for time-resolved measurements is set to a change in the cell voltage. The voltage of the fuel cell was changed between 0.4 V and 1.0 V (considered as OCV) or 0.4 V and 1.4 V, and currents for each measurement were recorded on the potentiostat in real time.

Our novel TG-QXAFS system uses the procedure shown in Figure 1 a: 1) a trigger signal is initially sent from the potentiostat; 2) after a time of T_1, the voltage of the in situ XAFS cell is stepped from one voltage (e.g. 0.4 V) to another voltage (e.g. 1.0 V); 3) a QXAFS measurement (15-s period) starts after a time of t_1, and thus, the delay time t can be defined as t_1-T_1, as shown in Figure 1 a. The delay time t is shifted at 1-s intervals, and a second QXAFS measurement is done. The procedure is repeated 15 times, and thus, a series of QXAFS spectra measured over a 15-s period is obtained. Then, its extended XAFS (EXAFS) oscillation in the range k is divided into 15 parts of 1-s intervals, and the 15 fragments of the EXAFS oscillations in 15 different measurements are combined together into one interval. Thus, we can obtain TG-QXAFS with a time resolution of 1 s, which is much faster than that (15 s) of the traditional QXAFS (Figure 1 a).

Figure 2 a, b shows a series of TG-QEXAFS oscillations at a Pt L_{III} edge for a Pt/C cathode catalyst during a voltage-stepped process from 1.0 V to 0.4 V and the Fourier transforms from 0.4 V to 1.0 V. All of the TG-QEXAFS spectra were resolved enough to use for EXAFS curve-fitting analysis in order to evaluate the numbers and lengths of chemical bonds on the Pt cathode catalyst every 1 s. This is the only in situ time-resolved study in which structural and electronic kinetics at a Pt/C fuel-cell catalyst with a time resolution of 1 s have been obtained while recording currents for each measurement on the potentiostat. Only a preceding study by time-resolved DXAFS, which is an alternative XAFS technique, has been reported; however, the time resolution was 10 s.[18] We have succeeded in observing the DXAFS for the Pt/C catalyst at 4-ms time resolution in this study.

Time-resolved analyses yielded four parameters: a) electrochemical charges of the fuel cell (potentiostat), b) the numbers and lengths of Pt–Pt bonds in the Pt nanoparticles, which reflect the particle size and stability of the Pt catalysts (EXAFS), c) those of Pt–O bonds, which provide details of the reactions between H_2O as well as O_2 and the Pt-particle surface (EXAFS), and d) the electron density of Pt d orbitals

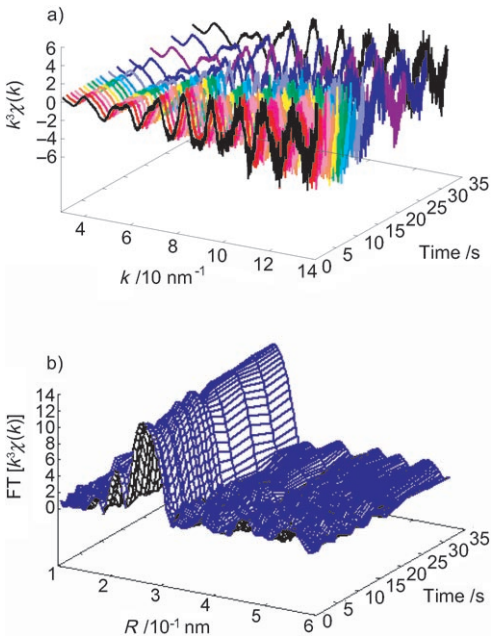

Figure 2. A series of TG-QEXAFS a) oscillations of a reduction process (1.0→0.4 V) and b) Fourier transforms of an oxidation process (0.4→1.0 V) at a Pt L_{III} edge in a Pt/C fuel cell measured at 333 K. Anode: H_2; cathode: N_2. Initial 15 s of each process was evaluated by TG-QXAFS with a gating time of 1 s. Middle of each process between 15 s and 30 s was measured by TG-QXAFS with a gating time of 5 s, and the data after 30 s were taken by the usual QXAFS every 15 s.

(XANES). Figure 3 shows the changes in these four parameters for both Pt reduction (voltage stepping: 1.0→0.4 V) and oxidation (0.4→1.0 V) processes on the Pt/C cathode catalyst under N_2 atmosphere. We have succeeded in determining the eight rate constants for the oxidation and reduction processes, respectively. The eight rate constants are related to the electron transfer, structural change, and d-electron density change at the Pt/C cathode catalyst, which are significantly different from each other. The TG-QXAFS analysis revealed a hysteresis loop for the structural changes in the Pt cathode particles in the oxidation and reduction processes.

All of the experimental results could be fitted with exponential curves. The changes in the coordination numbers (CN) of the Pt–Pt and Pt–O bonds, determined by TG-QEXAFS, and the d-electron density of state estimated by the peak area of QXANES measured every 2 s, were described with a single exponential function, indicating that the structural changes in the Pt particles follow first-order kinetics. Their rate constants are denoted as $k_{\text{Pt-Pt}}$ or $k'_{\text{Pt-Pt}}$, $k_{\text{Pt-O}}$ or $k'_{\text{Pt-O}}$, and k_d or k'_d for the oxidation or reduction processes, respectively. The electric changes were fitted with a linear combination of at least two exponential curves, from which k_{e1} or k'_{e1} and k_{e2} or k'_{e2} for the oxidation or reduction processes, respectively, were determined. Furthermore, the oxidation process required another term with linear dependence against reaction time, which seems to be a tiny steady-state oxidation of the carbon support (Ketjen EC).[19,20] These events on the cathode are illustrated in Figure 3e.

It should be noted that there is significant time lag between the four processes on the cathode surface as shown in Figure 3. In the oxidation process from 0.4 V to 1.0 V, all four elementary processes were much slower than those in the reduction process (Figure 3); however, the first dramatic electron transfer ($k_{e1} = 0.39\ s^{-1}$) was 8 times faster than the next process for the second electron transfer ($k_{e2} = 0.049\ s^{-1}$). After the first electron transfer, the Pt particles were only slightly charged, and there were no chemical bonds with oxygen on the Pt surface. Then Pt–O bonds slowly formed ($k_{\text{Pt-O}} = 0.013\ s^{-1}$) in conjunction with Pt charging with $k_d = 0.011\ s^{-1}$, which was monitored by the d-electron density of states (Figure 3e, gray line from left to right).

The CN of the Pt–Pt bonds remained constant at about 9 (Figure 3c) between 0.4–1.0 V, which indicates that decomposition of the Pt catalyst or significant leaching to the electrolyte did not occur. The CN of Pt–O bonds (0.4) under the steady-state condition of 1.0 V corresponds to a full monolayer of OH on the 2-nm Pt particles. In other words, the oxidation of the Pt particles by changing the potential from 0.4 V to 1.0 V occurs with the formation of Pt–OH covalent bonds on the surface of the Pt particles as shown in Figure 3e. The formation of adsorbed OH species in the oxygen reduction reaction above 0.8 V has also been previously proposed.[16,21–23]

The peak area of the Pt L_{III}-edge XANES, which has been shown to be related to the valence state of the Pt atom, can be used to estimate the variation in the electric charges. A large difference was observed between the amount of Pt charging and the electrochemical charge that flows at the electrode, as shown in Figure 3a. Similar behavior was also observed for the reverse process (Figure 3b). Hence, the rapid charge flow caused by voltage manipulation is not due to charging or discharging of the Pt catalysts but due to electron transfers at the interface between the Pt/C catalyst and the ionomer in the electric double layer (charging of the double layer). Electron transfer at the interface causes the activation of reactants (H_2O and O_2) on the surface of Pt particles in the fuel cell. A low-power-generation cathode catalyst using Pt particles of the same size (2 nm) exhibited not only poor electron transfer but also low Pt charging, which may stem from poor contact between the Pt particles and the carbon surface or the ionomer.

Although a similar time lag in the four elementary steps in the reduction processes was observed, the reduction processes had a different reaction mechanism (Figure 3e, black line from right to left). The first step was also a fast electron transfer (Figure 3b), for which the k'_{e1} value of 2.86 s^{-1} was 7.3 times higher than k_{e1} for the oxidation process. The second electron transfer ($k'_{e2} = 0.17\ s^{-1}$) occurred after Pt–O bond dissociation (reduction; $k'_{\text{Pt-O}} = 0.39\ s^{-1}$). The Pt–O bond dissociation process (probably a surface relaxation process) could be followed by our TG-QEXAFS with a time resolution of 1 s, whereas usual QXAFS with a time resolution of 15 s and energy-dispersive XAFS (DXAFS) with a time resolution of 10 s[18] can not monitor the reaction, because the chemical process is completed before the acquisition of one spectrum.

As the Pt–O bonds disappeared, the coordinated OH ions on the Pt surface accumulated electric charge from the Pt particles and the second electron transfer ($k'_{e2} = 0.17\ s^{-1}$) occurred, after the fast electron transfer at the interface in the

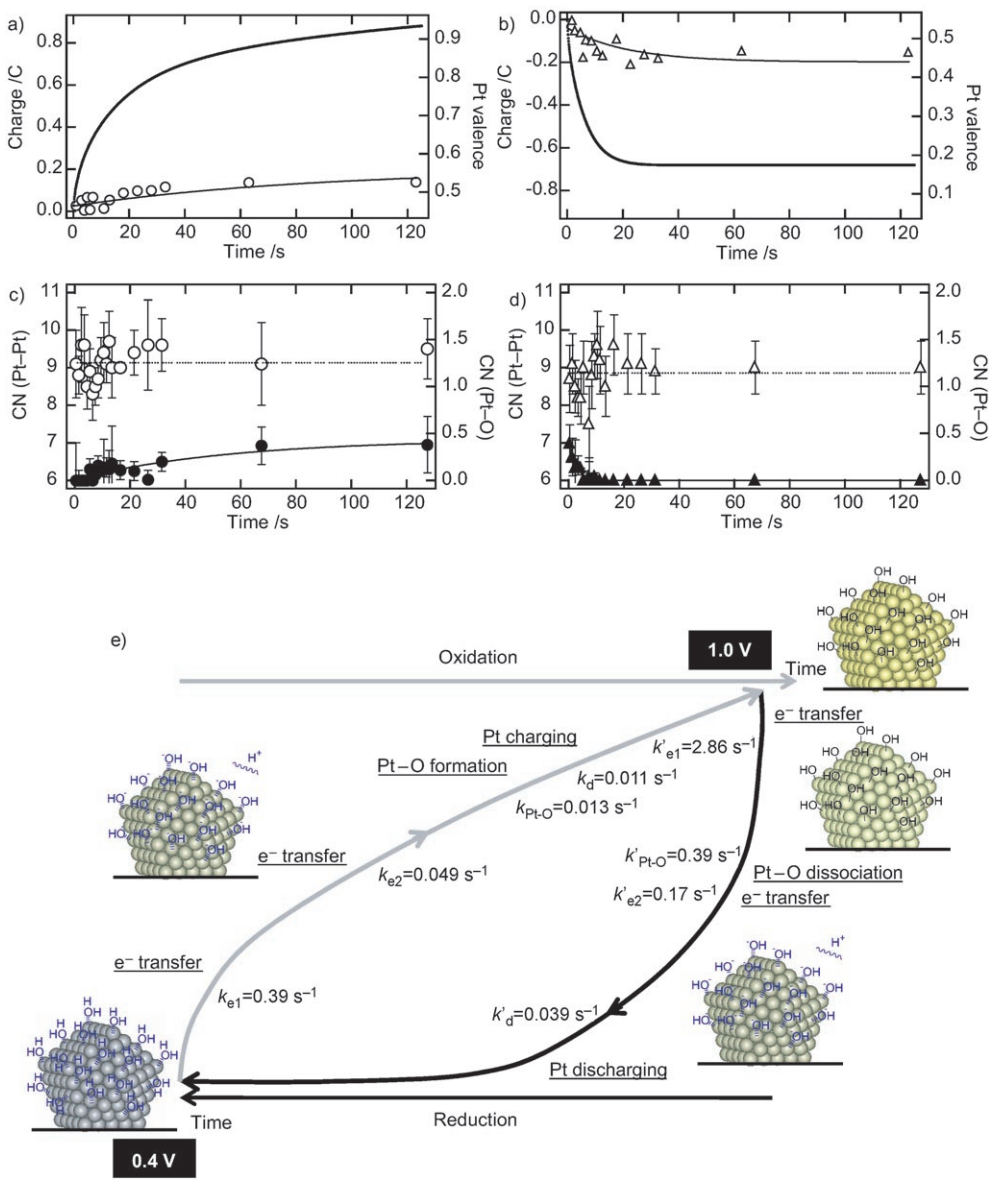

Figure 3. a, b) Changes in electric charges measured by a P/G stat (bold points) and those estimated by Pt L_{III}-edge TG-QXANES measured every 2 s (thin lines and marks); a) oxidation: 0.4→1.0 V; b) reduction: 1.0→0.4 V. Right axis is Pt valence estimated by QXANES, which corresponds to the electric charge presented on the left axis. Anode: H_2; cathode: N_2, 333 K. c, d) The coordination numbers of the Pt–Pt and Pt–O bonds measured by TG-QEXAFS; c) oxidation: 0.4→1.0 V; d) reduction: 1.0→0.4 V. Anode: H_2; cathode: N_2, 333 K; empty circles/triangles: Pt–Pt; filled circles/triangles: Pt–O. Initial 15 s of each process was evaluated by TG-QXAFS with a gating time of 1 s. Middle of each process between 15 s and 30 s was measured by TG-QXAFS with a gating time of 5 s, and the data after 30 s were taken by the usual QXAFS every 15 s. e) Reaction mechanism for changes in the Pt/C fuel-cell catalysts in cell voltages of 0.4/1.0 V under H_2 (anode) and N_2 (cathode) at 333 K. The kinetic parameters were obtained from the data measured by the potentiostat and time-gating QXAFS. H_2O adsorbed on the Pt surfaces at 0.4 V may be H_3O^+. The CN of Pt–Pt and Pt–O bonds represents the average number of Pt–Pt and Pt–O bonds, respectively, per Pt atom in the bulk catalyst.

electric double layer. Finally, Pt discharging finished (k'_d = 0.039 s^{-1}). Thus, the reduction process involves two different intermediate phases (Figure 3e), which demonstrates the structural hysteresis between the oxidation and reduction processes at the cathode. The CN of the Pt–Pt bonds, which indicates a cubo-octahedron nanostructure,[24] was also constant in the reduction process, as shown in Figure 3d. The Pt–Pt (0.276 nm) and Pt–O (0.200 nm) bond lengths remained unchanged during these processes.

When the cell voltage was increased to 1.4 V, which is higher than the OCV, the Pt particles were gradually oxidized. Similar oxidation of Pt catalysts was observed in the sweep of electrode potentials in H_2SO_4 and NaOH solutions.[13] The change in voltage from 0.4 V to 1.4 V caused a decrease in the CN of the Pt–Pt bonds and an increase in the CN of the Pt–O bonds. Their changes slowly occurred at similar rates (Figure 4a). The 20% decrease in the CN of the Pt–Pt bonds and the CN of 0.8 for the Pt–O bonds demonstrate that oxygen atoms enter the subsurface of the Pt particles at 1.4 V (Figure 4b). The k'_{Pt-O} (0.026 s^{-1}) and k'_{Pt-Pt} (0.031 s^{-1}) values were similar to each other, and were close to the k_{e2} value of 0.040 s^{-1}, indicating that Pt–O bond formation, Pt–Pt dissociation, and Pt charging occur simultaneously, as shown in Figure 4b. Then, slower Pt charging (k'_d = 0.010 s^{-1}) occurs. To examine whether there are other faster Pt charging processes, we monitored surface events by DXAFS with 4-ms time resolution (Supporting Information), which gave similar rates of Pt charging and discharging to those observed by the TG-QXAFS measurements, thus indicating that there are no other Pt valence-change processes.

Repeated voltage manipulations did not cause any decrease in electric charges, and the number of Pt–Pt bonds returned to its original value (9.0) when the cell voltage returned to 0.4 V. The oxygen that entered the subsurface of the Pt nanoparticles was released, and the Pt particles kept their cubo-octahedron structure. In other words, the Pt ions do not dissolve into the electrolyte under N_2 atmosphere,

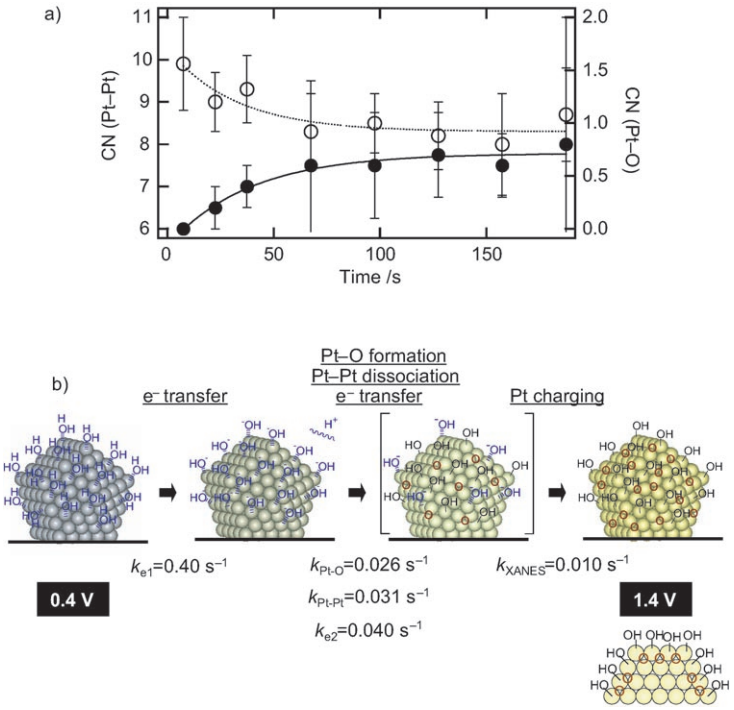

Figure 4. a) The coordination numbers of the Pt—Pt (empty circles) and Pt—O (filled circles) bonds measured every 15 s by the usual QXAFS for the oxidation process jumping from 0.4 V to 1.4 V. b) The structural model of the Pt nanoparticles suggested by in situ time-resolved QXAFS (The subsurface oxygen atoms should reconstruct the Pt surface, but it is not shown to avoid speculation for the reconstructed structure). Anode: H_2; cathode: N_2, 333 K. H_2O adsorbed on Pt surfaces at 0.4 V may be H_3O^+.

although the voltage (1.4 V) exceeds the threshold voltage for HO—H bond dissociation and promotes penetration of oxygen into the Pt subsurface.

In air, the bond behaviors at the cathode were completely distinct from those under the N_2 atmosphere. When the cell voltage was increased to 1.4 V, the Pt—Pt bonds immediately broke. The CN of the Pt—Pt bonds did not recover even if the cell voltage was returned to 0.4 V. If a local inclination of electric potential forms on electrode surfaces, dissolution of the Pt ions gradually occurs, resulting in serious deterioration of Pt cathode catalysts.

In conclusion, we have, for the first time, succeeded in the in situ time-resolved investigation of the reaction mechanisms occurring on the Pt/C catalyst surface in a fuel-cell cathode. A novel TG-QXAFS system was developed that enables real-time mechanistic investigation of electrocatalyst surfaces, and the reaction kinetics of the electron-transfer processes and redox structural changes, which involve eight elementary steps, on the Pt cathode catalysts were observed. Significant time lag between the electron transfer, the redox structural changes, and the Pt charging of the Pt/C catalysts is a characteristic property of Pt nanoparticles on a carbon support as well as the population of the bound OH species, which is crucial for the performance of a Pt/C catalyst in a fuel cell.

Experimental Section

Pt/C (Tanaka Kikinzoku Kogyo, Pt particle size: 2 nm (determined by TEM), Pt 50 wt%, 3.8 mg cm^{-2}) was used as a cathode catalyst, and Pt-free Pd/C (Tanaka Kikinzoku Kogyo, Pd 20 wt%, 0.5 mg cm^{-2}) was adopted as an anode catalyst. The MEA was stacked between the prepared XAFS cell in Figure 1c. H_2 (99.99%) for the anode, N_2 (99.99%) for the cathode, and dry air (cathode) were bubbled through deionized water baths at 323 K and heated at 333 K for introduction to the XAFS cell at 333 K. Gas pressures were ambient for all the gases and flow rates were controlled by mass-flow controllers before the water baths. The flow rates were regulated at 100 and 200 mL min^{-1} for anode and cathode, respectively. Heated gases with moisture entered into each electrode of the XAFS cell and reacted at the MEA. The gases were collected in bottles after the XAFS cell.

The XAFS cell was a seven-stacked structure (Figure 1c). The outer holder was made by a SUS 316 equipped with cartridge heaters, and the next current corrector made by Au-coated Cu was connected to the potentio/galvanostat (P/G stat). Insulator with epoxy resin was used as a separator of both electrodes. MEA was stacked between two grooved carbon flow channels and the gases were flowed between the grooves, which were in contact with the MEA. The details of in situ XAFS measurements and analysis are described in the Supporting Information.

Received: November 21, 2006
Revised: January 11, 2007
Published online: May 4, 2007

Keywords: electrochemistry · fuel cells · kinetics · reaction mechanisms · XAFS spectroscopy

[1] A. Z. Weber, J. Newman, *Chem. Rev.* **2004**, *104*, 4679.
[2] C. Y. Wang, *Chem. Rev.* **2004**, *104*, 4727.
[3] M. Z. Jacobson, W. G. Colella, D. M. Golden, *Science* **2005**, *308*, 1901.
[4] B. C. H. Steele, A. Heinzel, *Nature* **2001**, *414*, 345.
[5] *Electrocatalysis* (Eds.: J. Lipkowski, P. N. Ross), Wiley-VCH, New York, **1998**.
[6] Y. H. Huang, R. I. Dass, Z. L. Xing, J. B. Goodenough, *Science* **2006**, *312*, 254.
[7] V. Stamenkovic, B. S. Mun, K. J. J. Mayrhofer, P. N. Ross, N. M. Markovic, J. Rossmeisl, J. Greeley, J. K. Norskov, *Angew. Chem.* **2006**, *118*, 2963; *Angew. Chem. Int. Ed.* **2006**, *45*, 2897.
[8] Z. P. Shao, S. M. Haile, J. Ahn, P. D. Ronney, Z. L. Zhan, S. A. Barnett, *Nature* **2005**, *435*, 795.
[9] L. Zhang, S. Mukerjee, *J. Electrochem. Soc.* **2006**, *153*, A1062.
[10] P. J. Ferreira, G. J. Lao, Y. Shao-Horn, D. Morgan, R. Makharia, S. Kocha, H. Gasteriger, *J. Electrochem. Soc.* **2005**, *152*, A2256.
[11] A. E. Russell, A. Rose, *Chem. Rev.* **2004**, *104*, 4613.
[12] Y. H. Zhang, M. L. Toebes, A. van der Eerden, W. E. O'Grady, K. P. de Jong, D. C. Koningsberger, *J. Phys. Chem. B* **2004**, *108*, 18509.
[13] H. Yoshitake, T. Mochizuki, O. Yamazaki, K. Ota, *J. Electroanal. Chem.* **1993**, *361*, 229.
[14] *X-ray Absorption Fine Structure for Catalysts and Surfaces* (Ed.: Y. Iwasawa), World Scientific Publishing, Singapore, **1996**.
[15] C. Roth, H. Fuess, *Phys. Chem. Chem. Phys.* **2002**, *4*, 3555.
[16] V. S. Murthi, R. C. Urian, S. Mukerjee, *J. Phys. Chem. B* **2004**, *108*, 11011.
[17] W. S. Yoon, J. Hanson, J. McBreen, X. Q. Yang, *Electrochem. Commun.* **2006**, *8*, 859.

[18] P. G. Allen, S. D. Conradson, M. S. Wilson, S. Gottesfeld, I. D. Raistrick, J. Valcrio, M. Lovato, *J. Electroanal. Chem.* **1995**, *384*, 99.
[19] J. P. Meyers, R. M. Darling, *J. Electrochem. Soc.* **2006**, *153*, A1432.
[20] L. M. Roen, C. H. Paik, T. D. Jarvi, *Electrochem. Solid-State Lett.* **2004**, *7*, A19.
[21] A. K. N. Reddy, M. A. Genshaw, J. O'M Bockris, *J. Chem. Phys.* **1968**, *48*, 671.
[22] M. Teliska, V. S. Murthi, S. Mukerjee, D. E. Ramaker, *J. Electrochem. Soc.* **2005**, *152*, A2159.
[23] A. A. Pivovar, B. S. Pivovar, *J. Phys. Chem. B* **2005**, *109*, 785.
[24] R. E. Benfield, *J. Chem. Soc. Faraday Trans.* **1992**, *88*, 1107.

